*The Diffuse Interstellar Bands*
*Proceedings IAU Symposium No. 297, 2013*
*J. Cami & N. L. J. Cox, eds.*

doi:10.1017/S1743921313015834

# The Infrared Emission Bands

**E. Peeters**[1,2]

[1]Department of Physics and Astronomy, University of Western Ontario, London, ON N6A 3K7, Canada
email: epeeters@uwo.ca

[2]SETI Institute, 189 Bernardo Avenue, Suite 100, Mountain View, CA 94043, USA

**Abstract.** Up to 10% of the total power output of star-forming galaxies is emitted in the infrared emission features at 3.3, 6.2, 7.7, 8.6 and 11.2 $\mu$m. Here, I will review the spectral characteristics of these IR emission bands, their dependence on the local environment, the implications for the physical and chemical characteristics of the carriers, and their applicability as a diagnostic tool.

**Keywords.** infrared emission features, ISM: molecules, ISM: lines and bands, (stars:) circumstellar matter, infrared: general, astrochemistry

## 1. Introduction

In the early '70s, infrared (IR) detectors became available allowing the exploration of the IR universe. One of the many discoveries was the detection of strong, broad emission features at 8.6 and 11.2 $\mu$m and subsequently at 3.3, 6.2 and 7.7 $\mu$m (Fig. 1, e.g. Gillett *et al.* 1973; Russell *et al.* 1978). To date, these broad emission features are observed throughout the Universe in a wide variety of objects. These include post-AGB stars, planetary nebulae (PNe), HII regions, reflection nebulae (RNe), Herbig AeBe stars, the (diffuse) interstellar medium (ISM) and galaxies. In most cases, these IR emission features dominate the IR spectra of these objects. In fact, up to 10% of the total power output of star-forming galaxies is emitted in these infrared emission features (Smith *et al.* 2007).

The carrier of these IR emission bands remained unidentified for over a decade and so these bands were dubbed the unidentified IR (UIR) bands. A breakthrough came in the early '80s when one realized that the wavelengths of the IR emission bands coincide with the vibrational modes of carbonaceous material comprising aromatic units (Duley & Williams 1981). This resulted in a plethora of proposed candidate carriers, including Hydrogenated Amorphous Carbon (HAC, e.g. Duley & Williams 1983; Borghesi *et al.* 1987; Jones 2012), Quenched Carbon Composites (QCC, e.g. Sakata *et al.* 1984), Polycyclic Aromatic Hydrocarbons (PAHs, e.g. Allamandola *et al.* 1989; Puget & Léger 1989), Coal (e.g. Papoular *et al.* 1989), nanodiamonds (Jones & d'Hendecourt 2000), Rydberg matter (Holmlid 2000), Locally Aromatic Polycyclic Hydrocarbons (Petrie *et al.* 2003), and most recently mixed aromatic-aliphatic organic nano particles (MAONs, Kwok & Zhang 2011). All these candidates have one thing in common which is that they are comprised of aromatic units as it is exactly these aromatic units that give rise to the IR emission bands. They differ in properties such as the size (molecules, nano-particles, grains), the degree of aromaticity, the size of the aromatic units, and the exact carbonaceous structure. Amongst these candidates, PAHs are the prevailing carrier for the IR emission bands. This is largely based on two observations: i) the IR emission bands are observed towards RNe and in the ISM and ii) their colour temperature does not depend on the distance from the illuminating star of the RN. In these cold environment, classical dust grains do not attain sufficient high temperatures to emit at mid-IR wavelengths. Thus, these observations suggest that the carrier of the IR emission bands is able to

reach sufficiently high temperatures upon absorption of a single UV photon (Sellgren 1984). Hence, small species which have a limited heat capacity are required. For a PAH molecule, upon absorption of a UV photon, the molecule gets electronically excited. Internal redistribution of the energy leaves the molecule in a lower electronic state but highly vibrational excited. This highly vibrationally excited molecule then relaxes primarily via the emission of IR photons in their vibrational modes, resulting in the IR emission bands. In particular, the C-H stretching mode gives rise to the 3.3 $\mu$m band, the 6.2 $\mu$m band is due to C-C stretching vibrations, coupled C-C stretching and C-H in-plane bending vibrations result in the 7.7 $\mu$m feature, C-H in-plane-bending vibrations are located at 8.6 $\mu$m and the 10-15 $\mu$m region is due to C-H out-of-plane bending vibrations (Fig. 1).

It's important to realize that the carrier is not a single carrier but a family of species with similar structures. This immediately reveals one important limitation for the identification of the specific molecules as all these species have vibrational emission at roughly the same wavelengths in the mid-IR. This because the vibrational modes in the mid-IR are sensitive to the local molecular structure and not to the entire molecular structure of the species. Hence, no single PAH molecule has been firmly identified and thus the specifics of the PAH population remain unclear. Note however that when astronomers refer to PAH molecules, they do not use the strict chemical definition of PAHs but rather use this term for PAH and PAH-like species including PAHs with various side groups (e.g. $CH_3$), protonated PAHs, deuterated PAHs, PAHs which include hetero-atoms, PAHs with aliphatic bonds etc. While it's generally accepted that PAHs are the carriers of the IR emission bands (using this broad definition), recent papers by Kwok & Zhang (2011), Jones (2012) and Li & Draine (2012) exemplify the ongoing debate about the carriers. I will refer to the IR emission bands as PAHs bands in the remainder of the paper.

Since PAHs are seen throughout the Universe at high abundances, they are significant participants in several astrophysical and astrochemical processes. For example, they dominate the heating in the ISM through photo-electric ejection (Verstraete *et al.* 1990; Bakes & Tielens 1994). They influence the charge balance, and thus the gas-phase abundances in IS clouds through their effect on the equilibrium state of chemical reactions (Lepp & Dalgarno 1988; Bakes & Tielens 1998). In addition, they also affect surface chemistry through their large surfaces (Tielens *et al.* 1987) and may reduce the gas-phase D/H abundance (Draine 2004; Peeters *et al.* 2004a).

In this paper, I review the observational characteristics of the IR emission bands, their dependence on the local physical environment and highlight some implications for the characteristics of the carriers. In addition, I summarize how the IR emission bands are currently being used as a diagnostic tool.

Many papers have been written about these PAH bands. For further details, I refer in particular to reviews by Allamandola *et al.* (1989); Puget & Léger (1989); Tielens (2008) and the proceedings of "PAHs in the Universe" (Joblin & Tielens 2011).

## 2. Spectral Characteristics

Thanks to the improvement of IR detectors, the astronomical PAH spectrum is very rich and currently consists of the main features and a plethora of weaker emission features, located on large plateau emission bands (Fig. 1). These weaker features can include emission at 3.4, 3.5, 5.25, 5.75, 6.0, 6.6, 6.9, 7.2-7.4, 8.2, 10.5, 10.8, 11.0, 12.0, 12.7, 13.5, 14.2, 15.8, 16.4, 16.6, 17.0, 17.4 and, 17.8 $\mu$m. In addition, deuterated PAHs (PADs) are tentatively detected at 4.4 and 4.6 $\mu$m (Peeters *et al.* 2004a).

The exact decomposition of the PAH spectrum into its individual components is not unique and several methods are available (see e.g. Hony *et al.* 2001; Peeters *et al.* 2002;

https://doi.org/10.1017/S1743921313015834 Published online by Cambridge University Press

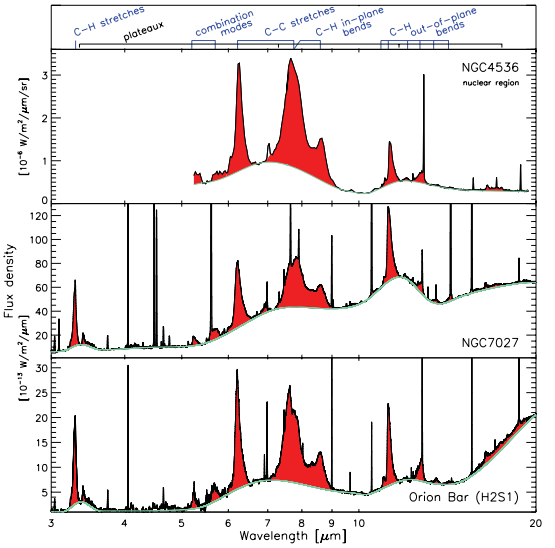


**Figure 1.** Typical PAH spectra: the ISO-SWS spectra of the planetary nebula NGC7027 and the Photo-Dissociation Region (PDR) at the Orion Bar and, the Spitzer-IRS spectrum of the nuclear region of NGC4536, an H II -type galaxy (Kennicutt *et al.* 2003). The mode identifications of the major PAH bands are indicated at the top. Figure taken from Peeters (2011).

Smith *et al.* 2007; Galliano *et al.* 2008; Tielens 2008; Peeters *et al.* 2012). The major differences are the adopted band profile and the treatment of the plateaus. In some methods, these plateaus are considered to be part of the individual features while in others they are considered to be independent features. None of the different decomposition methods is however technically correct (for a detailed discussion, see Tielens 2008). Clearly, the derived intensities of the individual features are highly dependent on the decomposition method. Fortunately, the overall results on the PAH characteristics and behaviour is independent of the decomposition method.

One of the most striking aspects of the astronomical PAH emission spectra is their similarity notwithstanding the large variety of environments in which they are observed. Indeed, to first order, the astronomical PAH spectrum is universal. Only when looking into detail does the diversity amongst the astronomical PAH spectra become apparent. This variation is reflected in the bands' positions, shapes and (relative) intensities from source to source and within extended sources.

## 3. Spectral Diversity

### 3.1. *Intensities*

Significant variations in the relative intensities of the IR emission bands have been observed in the Milky Way, the Magellanic Clouds and nearby galaxies within a sample of objects as well as spatially within extended sources. Several IR emission bands are found to correlate with each other, revealing their intimate connection (Fig. 2, e.g. Hony *et al.* 2001; Vermeij *et al.* 2002; Brandl *et al.* 2006; Sellgren *et al.* 2007; Smith *et al.* 2007; Galliano *et al.* 2008; Bernard-Salas *et al.* 2009; Acke *et al.* 2010; Sandstrom *et al.* 2010). The most established correlations are between the 3.3 and 11.2 $\mu$m bands and the 6.2, 7.7, 8.6 and 11.0 $\mu$m bands. Due to the high sensitivity of the Spitzer Space Telescope,

https://doi.org/10.1017/S1743921313015834 Published online by Cambridge University Press

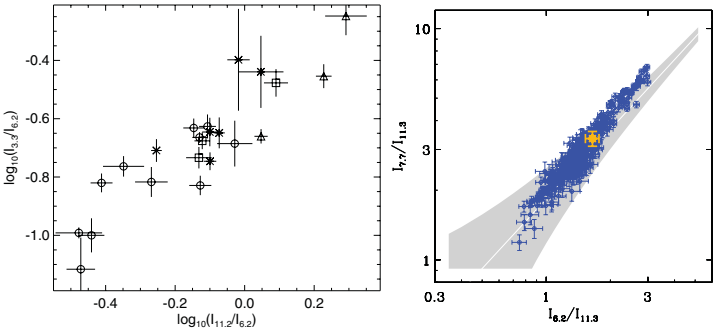


**Figure 2.** PAH intensity correlations. **Left:** The 3.3/6.2 vs the 11.2/6.2. H II regions are shown by ∘, intermediate mass star-forming regions by ×, RNe by □, PNe by △. Figure from Hony *et al.* (2001). **Right:** The 6.2/11.2 vs the 7.7/11.2 within the starburst galaxy M82. The white (gold) symbol represents the spectrum from the entire galaxy. The white line and the grey filled area (uncertainty) indicate the correlation obtained for the integrated spectra of a large sample of (extra-)galactic sources. Figure from Galliano *et al.* (2008).

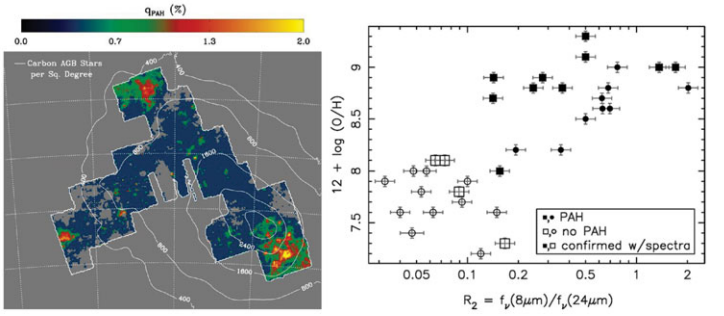


**Figure 3. Left:** Map of the fraction of the total dust mass contributed by PAHs with less than $10^3$ C atoms (qPAH). The contours represent the density of carbon stars per square degree. A similarity between the PAH fraction and the density of carbon stars is clearly lacking. Figure from Sandstrom *et al.* (2010). **Right:** Galaxy metallicity, expressed by 12 + log (O/H), as a function of the 8-to-24 $\mu$m colour representing the PAH/VSG ratio. Galaxies with or without PAH emission are clearly separated. Figure from Engelbracht *et al.* (2005).

these correlations studies are now extended to included the weaker IR emission bands (e.g. Boersma *et al.* 2010; Rosenberg *et al.* 2011; Peeters *et al.* 2012).

Exceptions to these well know correlations exist: two recent studies report that the 6.2 and 7.7 seem to decouple inside massive star forming regions (Whelan *et al.* 2013; Stock *et al.* 2013). In addition, weak or no 7.7 and 8.6 $\mu$m emission is observed towards some T-Tauri stars and HAeBe stars (Acke & van den Ancker 2004; Geers *et al.* 2006) and similarly, very weak emission in the 6 to 9 $\mu$m region relative to the 11.2 $\mu$m band intensity is observed towards several galaxies harboring an AGN (Kaneda *et al.* 2005; Smith *et al.* 2007; Bregman *et al.* 2008). Moreover, even when a set of features exhibit a very good correlation (with a very high correlation coefficient), the spatial distribution of these features may still show slight discrepancies (Peeters *et al.* 2013). Hence, spatial maps reveal subtleties missed by correlation plots.

Laboratory and theoretical studies of PAHs have shown that their intrinsic spectra depend on their charge, size, molecular (edge) structure and, temperature. Hence, the observed relative intensities in the PAH bands reflect the properties of the carrier which are, in turn, influenced by their environment as illustrated in the following two examples.

https://doi.org/10.1017/S1743921313015834 Published online by Cambridge University Press

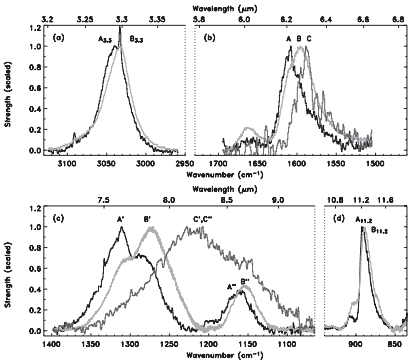


**Figure 4.** The variations in position and profile of the major PAH features represented by the different profile classes (Peeters *et al.* 2002, van Diedenhoven *et al.* 2004). Note that class B incorporates a range of profiles and hence a class B profile is not unique.

The main driver behind the most established correlations is the charge state of the carrier. Indeed, laboratory and theoretical PAH studies have long indicated that emission from neutral PAHs dominates at 3.3 and 11.2 $\mu$m while ionized PAHs emit strongest in the 5-10 $\mu$m and are responsible for the 11.0 $\mu$m band (e.g. Hudgins & Allamandola 2004, and reference therein). Likewise, observational studies of the observed intensity variations of the main PAH bands indicate they are primarily governed by the charge state (e.g. Joblin *et al.* 1996; Hony *et al.* 2001; Draine & Li 2001; Galliano *et al.* 2008).

The molecular edge structure is another characteristic of the emitting carrier that is revealed in the observed relative intensities. The edge structure determines the number of adjacent peripheral C-atoms bonded to an H-atom, which in turn, determines the frequency of the $CH_{oop}$ bending mode (e.g. Bellamy 1958; Hony *et al.* 2001). Hence, observations suggest that the carrier in planetary nebulae have very long smooth edges while H II regions harbour PAHs exhibiting more corners, either due to their smaller size or due to a more irregular structure.

Numerous studies also reveal significant variation in the total PAH intensity. Within extended Galactic H II regions, the PAHs to Very Small Grains (VSGs, determined around 15-25 $\mu$m) intensity ratio changes as the emission of VSGs dominates inside the H II region while the PAH emission dominates in the Photo-dissociation region (PDR; e.g. Lebouteiller *et al.* 2007; Churchwell *et al.* 2009). In a sample of spatially integrated H II regions, this PAH/VSGs ratio furthermore shows a dependence on the hardness of the radiation field (e.g. Gordon *et al.* 2008). A detailed study of the SMC reports that the spatial distribution of the fraction of the dust mass in PAHs, and hence the relative abundance of PAHs to dust, is clearly inhomogeneous (Fig. 3) and is correlated with that of the dust surface density and the molecular gas surface density but not with the carbon AGB star density (Sandstrom *et al.* 2010). These authors suggests that PAHs are formed in molecular clouds and/or destroyed in the ISM. A similar conclusion is reached when applying a mathematical decomposition of the PAH emission (see Sect. 4) while PAH destruction in the ISM is proposed for the formation of fullerenes (Berné & Tielens 2012). In addition, the relative abundance of PAHs to dust decreases with decreasing metallicity (Fig. 3; e.g. Engelbracht *et al.* 2005; Madden *et al.* 2006; Brandl *et al.* 2006; Galliano *et al.* 2008; Gordon *et al.* 2008; Calzetti 2011, and references therein). Whether this is due to enhanced PAH processing (destruction and/or modification of the PAHs by the hard radiation field) or due to a less efficient formation process is still under debate.

https://doi.org/10.1017/S1743921313015834 Published online by Cambridge University Press

### 3.2. *Profiles*

The profiles of the PAH emission bands can be fairly symmetric (e.g. 3.3 and 8.6 $\mu$m bands) or asymmetric. The latter appear as i) a steep blue wing and a red-shaded tail (e.g. 6.2 and 11.2 $\mu$m bands), ii) a steep red wing and a blue-shaded wing (12.7 $\mu$m band) or, iii) irregular which may arise from blending of multiple components (e.g. 7.7 $\mu$m complex). Like the PAH intensities, the profiles of the main PAH features exhibit clear variations from source to source and within sources, being most pronounced for the 7.7 $\mu$m complex (see Fig. 4; Cohen *et al.* 1989; Bregman 1989; Tokunaga *et al.* 1991; Peeters *et al.* 2002; van Diedenhoven *et al.* 2004). Each feature individually is classified in three major classes A, B and C, which is primarily based on their peak position (Tokunaga *et al.* 1991; Peeters *et al.* 2002; van Diedenhoven *et al.* 2004). While class A and C show only slight variations within their members, class B exhibit a wide range of profiles. Combined with the fact that some objects have band profiles encompassing two classes, this indicates that the band profiles show a continuous distribution with class A and C representing extremes in peak position and profile.

These profile variations are seen in the Milky Way and also in the Magellanic Clouds (e.g. Bernard-Salas *et al.* 2009; Matsuura *et al.* 2010) and show a dependence on object type and hence environment (Peeters *et al.* 2002; van Diedenhoven *et al.* 2004). Class A is associated with the ISM while class B and C is found towards circumstellar material (CSM). Furthermore, PAH studies within extended objects reveal that the band profiles depend on distance from the illuminating star and hence the local physical conditions (Fig. 5, Kerr *et al.* 1999; Tokunaga *et al.* 1991; Bregman & Temi 2005; Candian *et al.* 2012). The latter is exemplified by the dependence of the band profiles with the UV radiation field, G, and G/$n_e$ (with $n_e$ the electron density; Bregman & Temi 2005). Similarly, the band profiles show a dependence with the effective temperature, $T_{\rm eff}$, for a sample of post-AGB stars and isolated Herbig AeBe stars (Fig. 5, Sloan *et al.* 2005, 2007; Keller *et al.* 2008). However, this relationship with $T_{\rm eff}$ does not hold for planetary nebulae (very high $T_{\rm eff}$; class A and B) and reflection nebulae (low $T_{\rm eff}$; class A).

These band profiles variations originate primarily in a (chemical) modification of the emitting PAHs in different environments. The precise underlying modification is still under debate and various different processes are proposed. One should bear in mind though that the proposed modification also needs to satisfy the observed 'evolution' of the PAH classes through the PAH life cycle. In addition, comparison of the observed PAH classes with experimental and theoretical PAH spectra reveals another constraint as the class A 6.2 $\mu$m PAH is not reproduced by the strongest pure CC stretching mode of pure PAHs (Peeters *et al.* 2002; Hudgins *et al.* 2005). Here, I briefly list the proposed mechanisms and refer the reader to the listed papers for more details. Mechanisms specifically proposed for the class A 6.2 issue involve a small chemical change to the PAH molecule in order to invoke slight shifts in peak position of the vibrational modes. These include: i) Hetero-atom substituted PAHs (e.g. Peeters *et al.* 2002; Hudgins *et al.* 2005; Bauschlicher *et al.* 2009); ii) PAH-metal complexes (e.g. Hudgins *et al.* 2005; Bauschlicher & Ricca 2009; Simon & Joblin 2010; Joalland *et al.* 2009); iii) PAH clusters (e.g. Rapacioli *et al.* 2005; Simon & Joblin 2009). Mechanisms primarily invoked to interpret the different classes include the following: i) variations of the size distribution of the PAH family (Bauschlicher *et al.* 2008, 2009; Cami *et al.* 2011). Regarding the 7.7 $\mu$m complex, class A show a dominant 7.6 $\mu$m component attributed to small PAHs ($N_C \leqslant 48$; e.g. Peeters *et al.* 2002), class B a dominant component near 7.8-8 $\mu$m prominent in large PAHs ($54 \leqslant N_C \leqslant 130$ Bauschlicher *et al.* 2008, 2009) while class C profiles are reproduced by small PAHs (Cami *et al.* 2011); ii) variation of the degree of aromaticity (e.g. Sloan *et al.*

https://doi.org/10.1017/S1743921313015834 Published online by Cambridge University Press

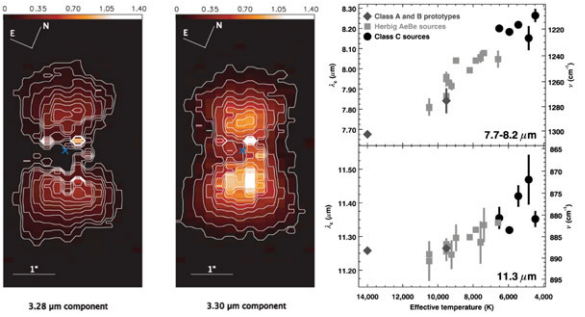


**Figure 5. Left:** The different spatial distributions of the two components (peaking at 3.28 and 3.3 $\mu$m) of the 3.3 $\mu$m IR emission band in the Red Rectangle. Figure taken from Candian *et al.* (2012). **Right:** The dependence of the central wavelength for the 7.7 and 11.2 IR emission band on effective temperature. Figure taken from Keller *et al.* (2008).

2007; Boersma *et al.* 2008; Keller *et al.* 2008; Pino *et al.* 2008; Acke *et al.* 2010; Carpentier *et al.* 2012; Kwok & Zhang 2011). The broad class C 7.7 $\mu$m complex is attributed to carbonaceous species with a low degree of aromaticity. UV processing (e.g. increasing $T_{\rm eff}$) preferentially breaks the aliphatic bands increasing the degree of aromaticity and hence resulting in an evolution towards a class B and then class A band profile. In order to apply this mechanism as well to YSOs, Boersma *et al.* (2008), proposed an active chemical equilibrium between aromatic and aliphatic species through hydrogenation, carbon reactions building (aliphatic) hydrocarbons and UV processing; iii) variation in the molecular edge structure (Candian *et al.* 2012). The variation in the 3.3 $\mu$m band profile is attributed to varying relative importance of bay and non-bay hydrogen sites.

## 4. Spectral decompositions

Using the full theoretically calculated NASA Ames PAH spectral database† (Bauchlicher *et al.* 2010, Boersma *et al.* 2013), very good fits are obtained using a non-negative-least-squares fitting approach to the observed PAH emission spectra (Cami *et al.* 2011, 2013). These fits are not unique and heavily biased by the content of the PAH database. Nevertheless, they confirm and reveal constraints on the PAH family responsible for individual PAH bands. For instance, the class A 6.2 $\mu$m band requires a large contribution of PANHs while the class B and C 6.2 $\mu$m band can be well reproduced by pure PAHs. Also, the 7.7 $\mu$m complex requires an increased relative fraction of small PAHs for its class A profile, an increase relative fraction of large PAHs for its class B profile and only small PAHs ($N_C \leqslant 30$) for its class C profile. This method is now further applied to extended sources to analyze the spatial behaviour of the PAH emission bands (Boersma *et al.* 2013; Bregman *et al.* 2013). A major result of these studies is the firm assignment of the 12.7 $\mu$m feature to ionized PAHs. This fitting method will be made available to the community in the near future (Boersma *et al.* 2013).

Another approach is the mathematical decomposition of PAH spectra within extended sources as a linear combination of a basis set of components which are spatially distinct (Boissel *et al.* 2001; Rapacioli *et al.* 2005; Berné *et al.* 2007, 2009, 2011; Rosenberg *et al.* 2011). A basis set of three components is found towards RNe and the edges of clouds. With increasing distance from the illuminating star, one finds ionized PAHs ($PAH^+$) followed by neutral PAHs ($PAH^0$), and then evaporating very small grains (eVSGs). This suggests the destruction of very small grains and/or PAH clusters under UV radiation

† http://www.astrochem.org/pahdb/

https://doi.org/10.1017/S1743921313015834 Published online by Cambridge University Press

resulting in PAH formation in the ISM. Due to the lack of spectral maps of class B and C objects, this three component basis set is expanded with 4 templates in order to fit the (spatially integrated) PAH emission towards these objects (Joblin *et al.* 2008).

## 5. PAH toolbox

Great progress has been made in recent years to use the PAH emission bands as a diagnostic tool. Several methods rely on the connection of the CC/CH ratio (i.e. the ratio of the 6.2 or 7.7 $\mu$m PAH band to the 3.3 or 11.2 $\mu$m PAH band) with the local physical conditions (e.g. Li & Draine 2001; Galliano *et al.* 2008). As discussed in Sect. 3.1, the CC/CH PAH ratio is dominated by a variation in the degree of ionization of the PAHs, which in turn, is governed by the ratio of the ionization rate to the recombination rate that is proportional to $G_0 T^{1/2}/n_e$ (with T the gas temperature, Tielens 2008). An estimate of the radiation field can also be found by applying PAHTAT (Pilleri *et al.* 2012). This method fit an astronomical spectrum with templates for the IR emission features, the eVSGs, atomic lines and continuum emission (see Sect. 4). It then relies on the strength of the eVSG in order to derive the radiation field.

In addition, the IR emission bands are particularly bright near sources of UV radiation, such as massive star-forming regions. Given their large abundance, the IR emission bands are thus a good tracer of star formation throughout the Universe (Calzetti 2011, and references therein). Indeed, star formation rates of galaxies are often obtained based on the strength of the IR emission bands. Likewise, they serve as diagnostics for the ultimate physical processes powering galactic nuclei (e.g. Genzel *et al.* 1998; Lutz *et al.* 1998; Peeters *et al.* 2004b; Sajina *et al.* 2007; Smith *et al.* 2007). Moreover, they can be used to determine redshifts in distant galaxies (e.g. Yan *et al.* 2007).

## 6. Conclusion

This paper presents the observational characteristics of the IR emission bands. Examples are given on how these characteristics can be used to enhance our understanding of their carriers and on how the IR emission bands can be used as a diagnostic tool.

Despite the progress made, several key issues remain: the complete identification of their carriers (i.e. specific molecules); the detection and characterization of the short and long wavelength counterparts of the IR emission bands; the formation, processing and destruction pathways, and hence their life cycle; the interaction between the molecule's characteristics (e.g. size, charge state) and the physical conditions of their environment (e.g. density, radiation field, temperature, metallicity) and related, the IR emission bands as a diagnostic probe of the physical conditions. In order to fully address these topics and make significant progress, an interdisciplinary effort, including theory, astronomical observations and laboratory studies and both physicists and chemists, is required.

### Acknowledgements

We thank C. Engelbracht, F. Galliano, S. Hony, L. Keller, K. Sandstrom and P. Sarre for providing figures for this article. Figures are reproduced by permission of the AAS, Royal Astronomical Society, ©ESO, and EDP sciences. This work was supported by an NSERC Discovery Grant.

### References

Acke, B., Bouwman, J., Juhász, A., *et al.* 2010, *ApJ*, 718, 558
Acke, B. & van den Ancker, M. E. 2004, *A&A*, 426, 151
Allamandola, L. J., Tielens, A. G. G. M., & Barker, J. R. 1989, *ApJS*, 71, 733

Bakes, E. L. O. & Tielens, A. G. G. M. 1994, *ApJ*, 427, 822
Bakes, E. L. O. & Tielens, A. G. G. M. 1998, *ApJ*, 499, 258
Bauschlicher, C. W., Peeters, E., & Allamandola, L. J. 2009, *ApJ*, 697, 311
Bauschlicher, Jr., C. W. & Ricca, A. 2009, *ApJ*, 698, 275
Bauschlicher, J. C. W., Peeters, E., & Allamandola, L. 2008, *ApJ*, 678, 316
Bellamy, L. 1958, The infra-red spectra of complex molecules, 2nd ed. (New York: John Wiley & Sons, Inc.)
Bernard-Salas, J., Peeters, E., Sloan, G. C., *et al.* 2009, *ApJ*, 699, 1541
Berné, O., Fuente, A., Goicoechea, J. R., *et al.* 2009, *ApJ*, 706, L160
Berné, O., Joblin, C., Deville, Y., *et al.* 2007, *A&A*, 469, 575
Berné, O., Pilleri, P., & Joblin, C. 2011, in EAS Publications Series, Vol. 46, EAS Publications Series, ed. C. Joblin & A. G. G. M. Tielens, 49–54
Berné, O. & Tielens, A. G. G. M. 2012, *Proceedings of the National Academy of Science*, 109, 401
Boersma, C., Bauschlicher, C. W., Allamandola, L. J., *et al.* 2010, *A&A*, 511, A32
Boersma, C., Bauschlicher, Jr., C. W., Ricca, A., *et al.* 2013, *ApJS*, submitted
Boersma, C., Bouwman, J., Lahuis, F., *et al.* 2008, *A&A*, 484, 241
Boissel, P., Joblin, C., & Pernot, P. 2001, *A&A*, 373, L5
Borghesi, A., Bussoletti, E., & Colangeli, L. 1987, *ApJ*, 314, 422
Brandl, B. R., Bernard-Salas, J., Spoon, H. W. W., *et al.* 2006, *ApJ*, 653, 1129
Bregman, J. 1989, in IAU Symp. 135: Interstellar Dust, Vol. 135, 109
Bregman, J., Boersma, C., Allamandola, L. *et al.* 2013, in prep.
Bregman, J. & Temi, P. 2005, *ApJ*, 621, 831
Bregman, J. D., Bregman, J. N., & Temi, P. 2008, in Astronomical Society of the Pacific Conference Series, Vol. 381, Infrared Diagnostics of Galaxy Evolution, ed. R.-R. Chary, H. I. Teplitz, & K. Sheth, 34
Calzetti, D. 2011, in EAS Publications Series, Vol. 46, EAS Publications Series, ed. C. Joblin & A. G. G. M. Tielens, 133–141
Cami, J., Bernard-Salas, J., Peeters, E., & Malek, S. E. 2011, in IAU Symposium, Vol. 280, IAU Symposium, 216–227
Cami, J., Boersma, C., Peeters, E. *et al.* 2013, in prep.
Candian, A., Kerr, T. H., Song, I.-O., McCombie, J., & Sarre, P. J. 2012, *MNRAS*, 426, 389
Carpentier, Y., Féraud, G., Dartois, E., *et al.* 2012, *A&A*, 548, A40
Churchwell, E., Babler, B. L., Meade, M. R., *et al.* 2009, *PASP*, 121, 213
Cohen, M., Tielens, A. G. G. M., Bregman, J., *et al.* 1989, *ApJ*, 341, 246
Draine, B. 2004, in Carnegie Observatories Astrophysics Series (eds) A. McWillian and M. Reach, Vol. 4, 0
Draine, B. T. & Li, A. 2001, *ApJ*, 551, 807
Duley, W. W. & Williams, D. A. 1981, *MNRAS*, 196, 269
Duley, W. W. & Williams, D. A. 1983, *MNRAS*, 205, 67P
Engelbracht, C. W., Gordon, K. D., Rieke, G. H., *et al.* 2005, *ApJ*, 628, L29
Galliano, F., Madden, S., Tielens, A., Peeters, E., & Jones, A. 2008, *ApJ*, 679, 310
Geers, V. C., Augereau, J.-C., Pontoppidan, K. M., *et al.* 2006, *A&A*, 459, 545
Genzel, R., Lutz, D., Sturm, E., *et al.* 1998, *ApJ*, 498, 579
Gillett, F. C., Forrest, W. J., & Merrill, K. M. 1973, *ApJ*, 183, 87
Gordon, K. D., Engelbracht, C. W., Rieke, G. H., *et al.* 2008, *ApJ*, 682, 336
Holmlid, L. 2000, *A&A*, 358, 276
Hony, S., Van Kerckhoven, C., Peeters, E., *et al.* 2001, *A&A*, 370, 1030
Hudgins, D. M. & Allamandola. 2004, in Astrophysics of Dust, ed. A. N. Witt, Astronomical Society of the Pacific, 000
Hudgins, D. M., Bauschlicher, Jr., C. W., & Allamandola, L. J. 2005, *ApJ*, 632, 316
Joalland, B., Simon, A., Marsden, C. J., & Joblin, C. 2009, *A&A*, 494, 969
Joblin, C., Szczerba, R., Berné, O., & Szyszka, C. 2008, *A&A*, 490, 189
Joblin, C. & Tielens, A. G. G. M., eds. 2011, EAS Publications Series, Vol. 46, PAHs and the Universe: A Symposium to Celebrate the 25th Anniversary of the PAH Hypothesis

Joblin, C., Tielens, A. G. G. M., Geballe, T. R., & Wooden, D. H. 1996, *ApJ*, 460, L119
Jones, A. P. 2012, *A&A*, 542, A98
Jones, A. P. & d'Hendecourt, L. 2000, *A&A*, 355, 1191
Kaneda, H., Onaka, T., & Sakon, I. 2005, *ApJ*, 632, L83
Keller, L. D., Sloan, G. C., Forrest, W. J., *et al.* 2008, *ApJ*, 684, 411
Kennicutt, Jr., R. C., Armus, L., Bendo, G., *et al.* 2003, *PASP*, 115, 928
Kerr, T. H., Hurst, M. E., Miles, J. R., & Sarre, P. J. 1999, *MNRAS*, 303, 446
Kwok, S. & Zhang, Y. 2011, *Nature*, 479, 80
Lebouteiller, V., Brandl, B., Bernard-Salas, J., Devost, D., & Houck, J. R. 2007, *ApJ*, 665, 390
Lepp, S. & Dalgarno, A. 1988, *ApJ*, 324, 553
Li, A. & Draine, B. T. 2001, *ApJ*, 554, 778
Li, A. & Draine, B. T. 2012, *ApJ*, 760, L35
Lutz, D., Spoon, H. W. W., Rigopoulou, D., Moorwood, A. F. M., & Genzel, R. 1998, *ApJ*, 505, L103
Madden, S. C., Galliano, F., Jones, A. P., & Sauvage, M. 2006, *A&A*, 446, 877
Matsuura, M., Sloan, G. C., Bernard-Salas, J., *et al.* 2010, ArXiv 1011.1579
Papoular, R., Conrad, J., Giuliano, M., Kister, J., & Mille, G. 1989, *A&A*, 217, 204
Peeters, E. 2011, in EAS Publications Series, Vol. 46, EAS Publications Series, ed. C. Joblin & A. G. G. M. Tielens, 13–27
Peeters, E., Allamandola, L. J., Bauschlicher, C. W., *et al.* 2004a, *ApJ*, 604, 252
Peeters, E., Hony, S., Van Kerckhoven, C., *et al.* 2002, *A&A*, 390, 1089
Peeters, E., Spoon, H. W. W., & Tielens, A. G. G. M. 2004b, *ApJ*, 613, 986
Peeters, E., Tielens, A. G. G. M., Allamandola, L. J., *et al.* 2013, in prep.
Peeters, E., Tielens, A. G. G. M., Allamandola, L. J., & Wolfire, M. G. 2012, *ApJ*, 747, 44
Petrie, S., Stranger, R., & Duley, W. W. 2003, *ApJ*, 594, 869
Pilleri, P., Montillaud, J., Berné, O., & Joblin, C. 2012, *A&A*, 542, A69
Pino, T., Dartois, E., Cao, A.-T., *et al.* 2008, *A&A*, 490, 665
Puget, J. L. & Léger, A. 1989, *ARA&A*, 27, 161
Rapacioli, M., Joblin, C., & Boissel, P. 2005, *A&A*, 429, 193
Rosenberg, M. J. F., Berné, O., Boersma, C., Allamandola, L. J., & Tielens, A. G. G. M. 2011, *A&A*, 532, A128
Russell, R. W., Soifer, B. T., & Willner, S. P. 1978, *ApJ*, 220, 568
Sajina, A., Yan, L., Armus, L., *et al.* 2007, *ApJ*, 664, 713
Sakata, A., Wada, S., Tanabe, T., & Onaka, T. 1984, *ApJ*, 287, L51
Sandstrom, K. M., Bolatto, A. D., Draine, B. T., Bot, C., & Stanimirović, S. 2010, *ApJ*, 715, 701
Sellgren, K. 1984, *ApJ*, 277, 623
Sellgren, K., Uchida, K. I., & Werner, M. W. 2007, *ApJ*, 659, 1338
Simon, A. & Joblin, C. 2009, Journal of Physical Chemistry A, 113, 4878
Simon, A. & Joblin, C. 2010, *ApJ*, 712, 69
Sloan, G. C., Jura, M., Duley, W. W., *et al.* 2007, *ApJ*, 664, 1144
Sloan, G. C., Keller, L. D., Forrest, W. J., *et al.* 2005, *ApJ*, 632, 956
Smith, J. D. T., Draine, B. T., Dale, D. A., *et al.* 2007, *ApJ*, 656, 770
Stock, D. J., Peeters, E., & Choi, D. Y. Bik, A. 2013, *ApJ*, submitted.
Tielens, A. G. G. M. 2008, *ARA&A*, 46, 289
Tielens, A. G. G. M., Allamandola, L. J., Barker, J. R., & Cohen, M. 1987, in Polycyclic Aromatic Hydrocarbons and Astrophysics, 273
Tokunaga, A. T., Sellgren, K., Smith, R. G., *et al.* 1991, *ApJ*, 380, 452
van Diedenhoven, B., Peeters, E., Van Kerckhoven, C., *et al.* 2004, *ApJ*, 611, 928
Vermeij, R., Peeters, E., Tielens, A. G. G. M., & van der Hulst, J. M. 2002, *A&A*, 382, 1042
Verstraete, L., Leger, A., D'Hendecourt, L., Defourneau, D., & Dutuit, O. 1990, *A&A*, 237, 436
Whelan, D. G., Lebouteiller, V., Galliano, F., *et al.* 2013, *ApJ*, 771, 16
Yan, L., Sajina, A., Fadda, D., *et al.* 2007, *ApJ*, 658, 778